Available online at www.sciencedirect.com
ScienceDirect
Trans. Nonferrous Met. Soc. China 27(2017) 1725−1734
Transactions of Nonferrous Metals Society of China
www.tnmsc.cn

A comparative study on corrosion of Mg−Al−Si alloys

Sennur CANDAN[1], Ercan CANDAN[2]

1. Department of Mechanical and Manufacturing Engineering, Bilecik Seyh Edebali University, Bilecik 11210, Turkey;
2. Department of Mechanical Engineering, Avrasya University, Trabzon 61200, Turkey

Received 19 May 2016; accepted 10 September 2016

Abstract: Corrosion behavior of various Mg−Al−Si alloys (AS11, AS21, AS41, AS61 and AS91 series), cast under the same cooling conditions and controlled alloying composition, was investigated systematically. Optical microscopy and scanning electron microscopy were used for microstructural examinations. The corrosion behavior was evaluated by immersion tests and potentiodynamic polarization measurements in 3.5% NaCl solution. The results from both immersion tests and the potentiodynamic polarization measurements showed that marginal improvement in corrosion resistance was observed with 2.0% Al (mass fraction) containing alloy (AS21) whereas Al addition above 2.0% (AS41, AS61 and AS91) deteriorated the corrosion resistance which was attributed to β phase, acting as cathode, and the interruption of continuity of the oxide film on the surface of the alloys owing to coarsened β and Mg_2Si phases.

Key words: Mg alloy; AS series alloys; microstructure; corrosion

1 Introduction

Aluminum containing magnesium alloys (AZ, AM, AS series) are particularly attractive for aerospace and automotive industries due to their low densities [1−4]. Si addition to Mg alloys enhances the fluidity of the molten metal, therefore improves their casting properties. The binary Mg−Si phase diagram [5] presents the formation of Mg_2Si intermetallic having high melting point of around 1100 °C. This intermetallic phase is very stable which pins grain boundaries and hinders both grain boundary migration and sliding at elevated temperatures [6]. Thus, Mg−Al−Si based alloys (AS series Mg alloys) have high potential as heat resistant light metals. AS series Mg alloy systems are already in use for automotive industry due to their high creep resistance [4]. For example, parts made from AS21 and AS41 alloys, have been successfully used in the automobile engines [1,4].

In the last few years, numerous studies have been conducted on AS series alloys to understand their creep mechanisms at elevated temperatures [6−10] and their machinability [11]. Given the nature of the application environment, corrosion resistance also is an important parameter as well as creep resistance of the Mg alloys. However, studies on corrosion behavior of AS series Mg alloys, published in the journals, are scarce [12−15]. SENF et al [12] reported the corrosion behavior of AS41, AZ91, AM60 and AE42 alloys. Looking at their results, under the salt spray conditions, AE42 showed the best corrosion behavior followed by AZ91 and AM60 while corrosion attack at the samples made of AS41 was tremendous. ZUCCHI et al [13] reported the corrosion behavior of both heat treated and untreated AS21 alloys under sulphate and chloride environment. They reported that the grains of AS21 alloys were composed of Mg-rich solid solution (α-phase), while the grain boundary region was composed of $Mg_{17}Al_{12}$ (β) intermetallic phase and silicon-rich phase (Mg_2Si). Most recently, ELSAWY et al [14] compared corrosion behavior of AS31 and AZ91 alloys on the effect of nitrates in the presence and the absence of buffers (phosphate and borate). When phosphate buffer was used, a protective layer of magnesium phosphate has formed. The rate of formation of such protective layer has been found to increase with increasing both nitrate concentration and aluminum content in the alloy.

Although, aforementioned studies [12−15] above dealt with corrosion behaviors of AS series Mg alloys, these studies were carried out in a non-systematic manner. For example, AS31 or AS41 was compared with AZ91 alloy [12,14] and discussed in the frame of its Al

Corresponding author: Ercan CANDAN; E-mail: ecandan@yahoo.com
DOI: 10.1016/S1003-6326(17)60195-X

content, ignoring the Zn in AZ series alloys. It is well known that alloying elements [16−20] and cooling conditions [21,22] overwhelmingly affect the microstructure and therefore the corrosion resistance of the Mg alloys. Thus, this study aimed a comparative investigation on the corrosion of various AS series Mg alloys (AS11, AS21, AS41, AS61 and AS91) cast under the same cooling conditions and controlled alloying composition.

2 Experimental

The magnesium alloys were prepared by melting pure Mg, Al, and Al−Si master alloy (Al−12%Si, mass fraction) in a graphite crucible under argon gas (Ar) atmosphere at 750 °C. The samples were obtained by casting of the molten alloys into a cast iron mold under protective SF_6 gas. The mould was preheated to 250 °C prior to the casting. The alloy specimens were used in as-cast condition. The chemical compositions of the alloys, determined by optical emission spectrometry (OES), are given in Table 1.

Table 1 Chemical compositions of AS series magnesium alloys used (mass fraction, %)

Alloy	Al	Mn	Zn	Si	Mg
AS11	1.19	0.19	0.11	1.12	Rest
AS21	2.13	0.23	0.13	1.10	Rest
AS41	3.87	0.16	0.16	1.15	Rest
AS61	5.90	0.19	0.14	1.16	Rest
AS91	9.21	0.25	0.18	1.10	Rest

Microstructural evaluations were carried out by optical microscopy (OM) and scanning electron microscopy (SEM). Samples having approximately 9 mm × 9 mm × 15 mm dimesions were cut and subsequently ground from 220 to 1200 grit emery papers followed by polishing with 1 μm diamond paste for the immersion tests and microstructural evaluations. For SEM investigations of AS11, AS21 and AS41, polished samples were etched with a solution consisting of 10% HNO_3 in alcohol then further etched in acetic-picral for a few seconds. For AS61 and AS91 alloys, 3% HNO_3 in alcohol was used as an etchant.

Two different immersion tests were employed: one was for corrosion loss measurements and the other was for observation of initial stage of the oxide film on the surface of the samples. The polished samples were weighed and then immersed in 3.5% NaCl solution for 72 h for the corrosion loss measurements. After the immersion tests, the samples were cleaned with a solution containing 200 g/L CrO_3 for 15 min to remove the corrosion products. Finally, they were cleaned with distilled water, dried and weighed. The corrosion losses of the samples were then normalized in the unit of mg/(cm^2·d) by considering the total surface area of the samples. For the observation of the oxide film, the polished samples were immersed in 3.5% NaCl solution for 1 h then ultrasonically cleaned in distilled water and left to dry at room temperature.

For the potentiodynamic polarization measurements, machined samples of 9 mm × 9 mm × 9 mm were connected to copper wire and embedded in an epoxy resin holder. The surfaces were then abraded up to 1200 grit emery paper, mechanically polished down to 1 μm diamond paste and washed and ultrasonically rinsed in distilled water. The potentiodynamic curves were performed by means of a Gamry model PC4/300 mA potentiostat/galvanostat controlled by a computer with DC105 corrosion analysis software. The embedded specimens in epoxy resin were utilized as working electrodes. A carbon rod (6 mm in diameter) and a saturated calomel electrode (SCE) were used as a counter electrode and reference electrode, respectively. Experiments were performed at room temperature in a glass cell containing 3.5% NaCl solution. Each polarization experiment was carried out holding the electrode for 45 min at open circuit potential (E_o) to allow steady-state to be achieved. Potentiodynamic polarization curves were generated by sweeping the potential from cathodic to anodic direction at a scan rate of 1 mV/s, starting from −2.00 up to 0.20 V. Each data point for both immersion and potentiodynamic polarization tests represents at least average of 3 different measurements.

3 Results and discussion

3.1 Microstructure

The microstructures of the examined AS series Mg alloys are shown in Figs. 1(a)–(e). It was observed that the microstructure consisted of primarily Mg-rich solid solution and secondary intermetallic phases both in the grain boundaries and occasionally within the α-Mg grains. Presence of the secondary intermetallic phases increased in an increasing order in AS11, AS21, AS41, AS61 and AS91 alloys (see Figs. 1(a)−(e)). High magnification SEM images and EDS analysis of AS21 and AS91 alloys are shown in Figs. 2(a) and (b), respectively. The EDS micro analysis in Fig. 2(a) confirms that the second phase particles with a globular shape (marked as 1 and 3) contain mainly Mg−Al−Mn elements and continuous phase alongside the grain boundaries contain Mg−Si elements (marked as 2). EVANGELISTA et al [8] reported that the secondary phases at grain boundaries of AS21 alloy mainly

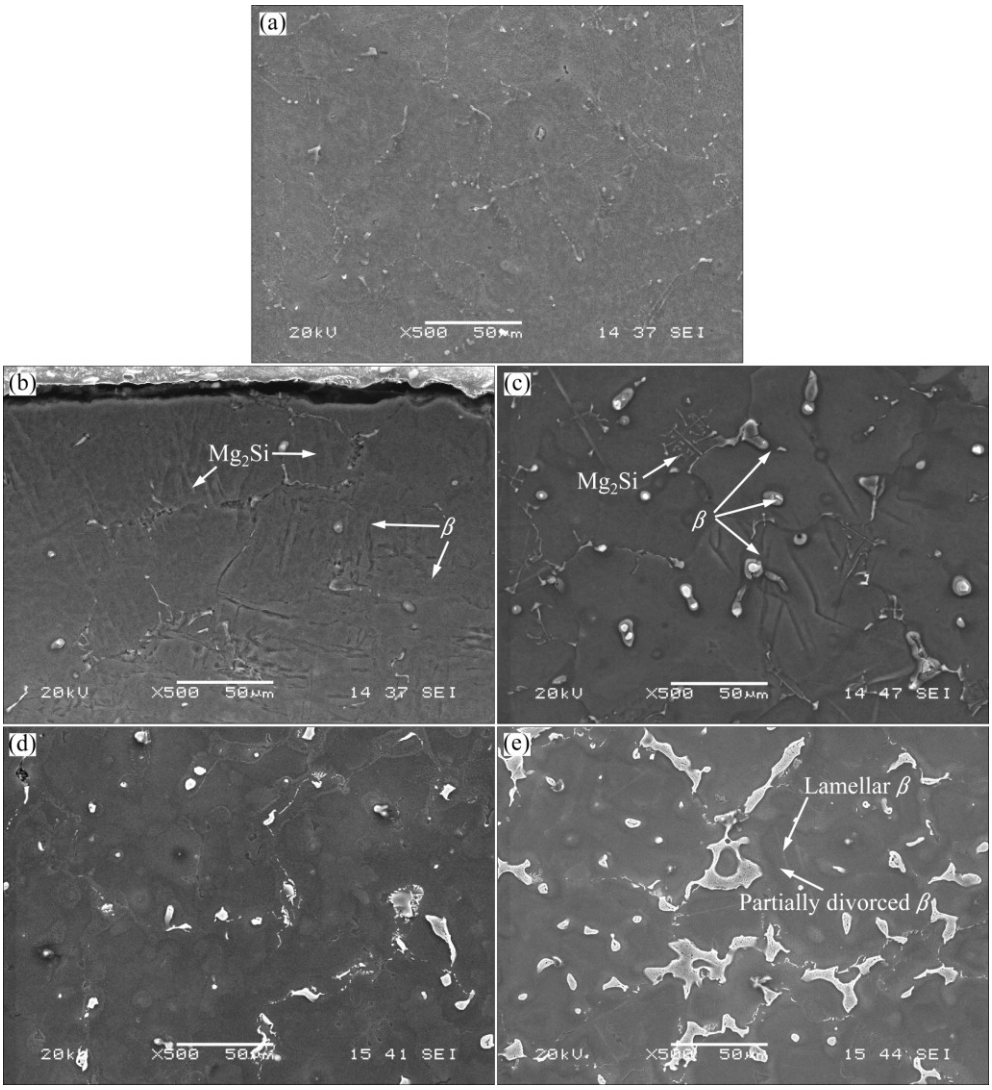

Fig. 1 SEM images showing microstructures of AS11 (a), AS21 (b), AS41 (c), AS61 (d) and AS91 (e) series Mg alloys

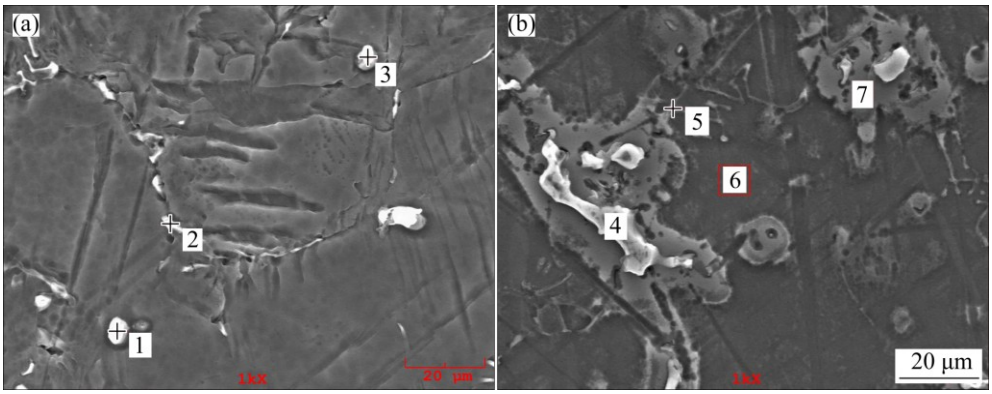

Location	1	2	3	4	5	6	7
Al	32.1	1.2	29.5	37.2	3.7	1.3	10.5
Si	0.6	28.2	0.8	−	11.9	−	−
Mn	4.1		4.8	−	−	−	−
Mg	63.1	70.5	64.8	62.3	84.3	98.6	89.5

Fig. 2 SEM images of AS21 (a) and AS91 (b) alloys (The numbers indicated on micrographs represent places where EDS measurement was carried out)

consisted of Mg_2Si and $Mg_{17}Al_{12}$ (β) intermetallic phases. They reported that [8] the Mg_2Si phases had Chinese script or blocky aspect and the β had low amount and globular shape in accord with the present work. Additionally, RUDAJEVOVÁ and LUKÁČ [10], PEKGULERYUZ and KAYA [23] or BRONFIN et al [24] consistently reported that the amount of β in AS21 alloy was negligible in agreement with the present work. According to the Mg−Al equilibrium phase diagram, the eutectic β is expected to appear when the Al content reaches ~13% (mass fraction). However, the eutectic β phase appears in alloys containing above 2% Al in nonequilibrium cooling conditions normally encountered in Mg alloy castings [25,26]. The globular shape β phase was transformed into a more coarsened morphology when the Al content of the alloys increased (see Figs. 1(c)–(e)). As shown in Figs. 1(d) and (e), lamellar and partially divorced β eutectic appears in higher Al containing alloys (i.e., AS61 and AS91 alloys), the latter was more pronounced in the AS91 alloy. The EDS microanalysis in Fig. 2(b) indicated that the Al content of the lamellar β eutectic (marked as 7) was 10.5% while it was 37.2% (mass fraction) in the partially divorced β eutectic (marked as 4). It should be noted that the contrast difference between the lamellar and partially divorced β eutectics are due to etchants used. It is well known [16,17,22,27] that the β eutectic is of divorced, partially divorced and lamellar structure in AZ91 alloy which contains ~9% Al (mass fraction). As reported previously [16,17,22,27], the eutectic with the lamellar structure in AZ91 Mg alloy is formed adjacent to the partially divorced eutectics in accord with the present work.

Optical microscopy images of Mg_2Si phases present in the AS21 and AS91 alloys are shown in Figs. 3(a) and (b), respectively. In agreement with Refs. [8,10,28], the Mg_2Si phase had formed in two different morphologies: as Chinese-script type and as dispersed blocky particles. The majority of them are of the Chinese-script type. It was noted that the Mg_2Si intermetallic phases dispersed as fine particles and needle-like Chinese-script in the microstructure of AS11 and AS21 alloys whereas these phases appeared as blocky particles and bold Chinese-script type intermetallics as Al content increased in the alloys (i.e., AS41, AS61 and AS91, respectively). This phonemenon was attributed to the effect of Al on the microstrcture of Mg alloy. ZHENG et al [29] studied the effects of different amounts of Al (1% to 9%) on the microstructure and properties of Mg−Al binary alloys. They reported that α-Mg dendrites convert from a columnar structure to an equiaxial structure as small as 1.0% Al added to Mg. They explained this phenomenon as: with increasing Al content, α-Mg dendrites become more developed, and the dendrite arms become finer. When Al is added to Mg, the stable Al solute-rich layer is built up in front of the solidification interface, resulting in the formation of a constitutional super-cooling zone, which destroys the original planar interface and forms the dendrites. With an increase in the Al content, the degree of solute enrichment increases, and this decreases the super-cooling. As a consequence, it suppresses the growth of α-Mg dendrites and results in the refinement of α-Mg dendrite arms. Since Si is practically insoluble in magnesium [5], transformation of dendrites from columnar to exuiaxed dendrite structure, owing to Al addition, may result in higher segregation of Si in certain areas, leading to a formation of blocky particles and/or bold Chinese-script type Mg_2Si intermetallics. Indeed, the amount of Si content in the α-Mg matrix is reduced when Al content of the alloy increases as shown in Table 2, supporting the discussion.

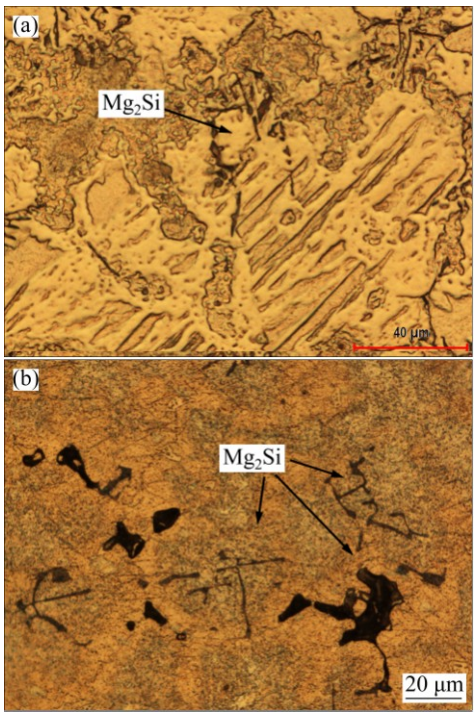

Fig. 3 Optical micrographs showing presence of Mg_2Si phase in AS21 (a) and AS91 (b) alloys

Table 2 Al and Si contents in α-Mg of AS series alloys obtained by EDS analysis

Alloy	w(Al)/%	w(Si)/%
AS11	0.96	0.83
AS21	1.41	0.46
AS41	1.70	0.10
AS61	3.92	0.07
AS91	4.61	0.06

3.2 Corrosion

Figures 4(a)−(e) present macroscopic photographs of the corroded samples which were exposed in 3.5% NaCl solution for 72 h. In AS11 and AS21 alloys (see Figs. 4(a) and (b)), most of the surface only suffer punctate corrosion lightly while in AS41, AS61 and AS91 alloys (Figs. 4(c)−(e)), the whole surface suffered from severe corrosion and samples have been dissolved basically. Figure 5 illustrates the results of corrosion loss from the immersion tests. The corrosion loss was calculated by the proportioning of the mass change before and after corrosion to the sample surface area (mg/(cm^2·d)). Evidently, corrosion loss of the samples increased abruptly with increasing their Al content above 2%. It was noted that the corrosion loss values of AS11 and AS21 alloys are close (2.5 and 1.4 mg/(cm^2·d), respectively) whereas the corrosion loss increased dramatically as the Al content of the alloys increased (i.e., 18.6, 31.8 and 54.5 mg/(cm^2·d) for AS41, AS61 and AS91 alloys, respectively).

Cross section SEM images of the samples, immersed in 3.5% NaCl for 72 h, are shown in Figs. 6(a)−(e). The corrosion had propagated from the surface through inner part of the alloy, and many deep corrosion pits on the surface of the alloys took place. Evidently, AS11 and AS21 alloys exhibited much better corrosion resistance compared with those of the AS41, AS61 and AS91, indicating that the alloys containing higher Al contents (>2.0%), are subjected to a higher localized breakdown. The corrosion attack at the samples made of AS91 is tremendous under immersion test conditions. The significance of Fig. 6(e) is that the

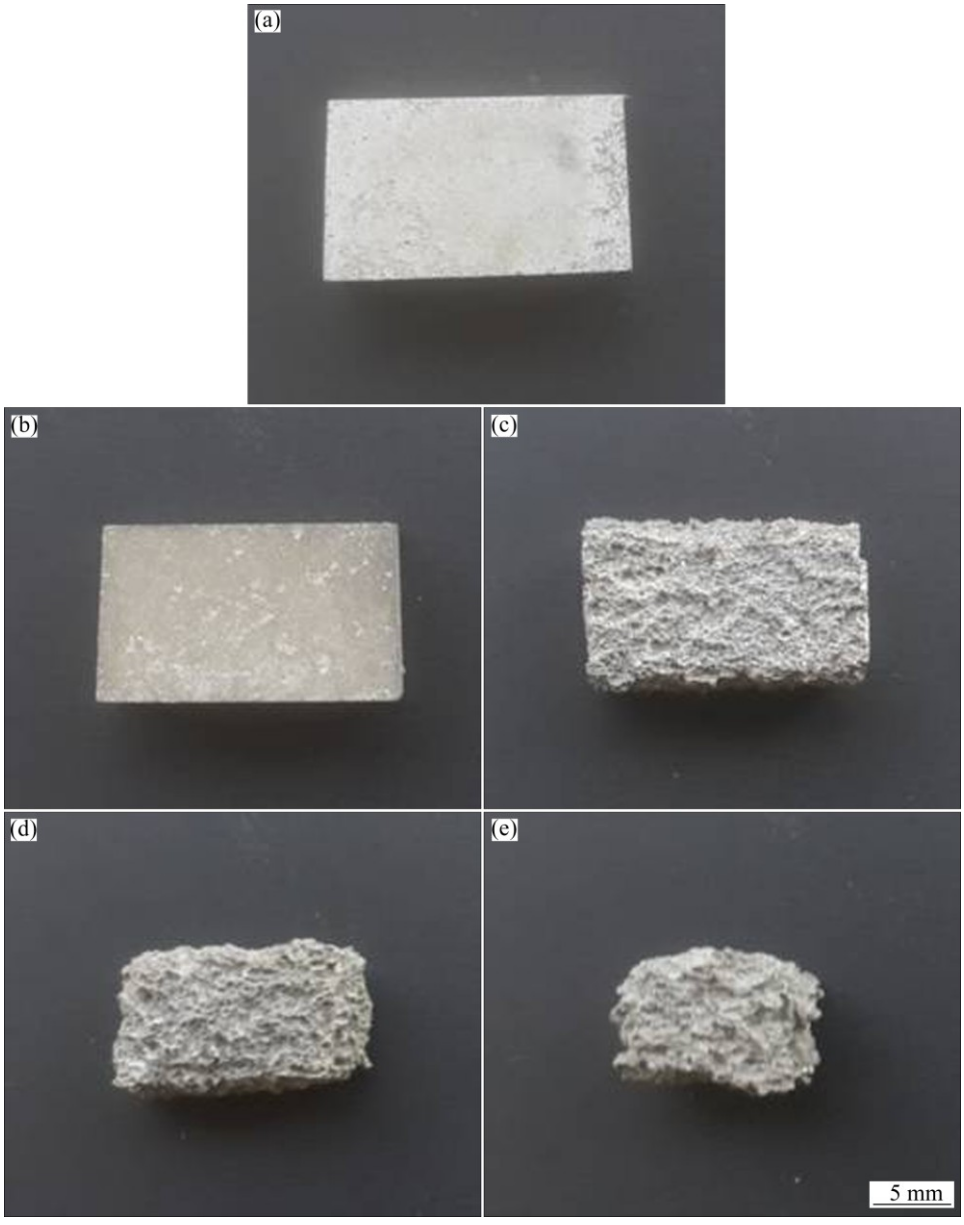

Fig. 4 Macroscopical pictures of AS11 (a), AS21 (b), AS41 (c), AS61 (d) and AS91 (e) alloys exposed to 3.5% NaCl for 72 h

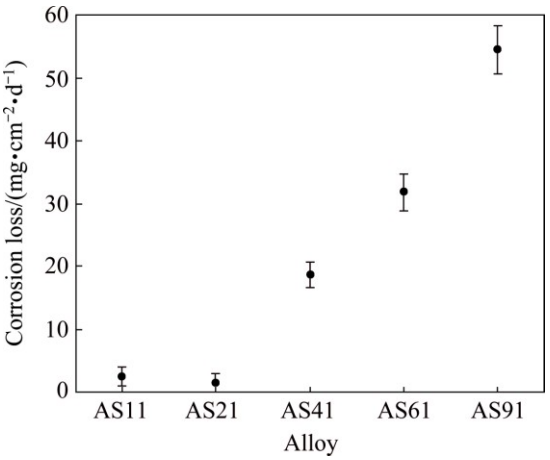

Fig. 5 Corrosion loss of AS series Mg alloys from immersion tests

corrosion had been propagated through inner part of the AS91 alloy by following the β phase network. Depending on its extend and morphology, the role of β phase as an effective barrier or active cathode in AZ series Mg alloys, have been reported in Refs. [29,30]. It acts as an effective barrier if its volume fraction is high and the interparticle distance is sufficiently close like in pressure die cast alloys [27,30−32]. On the other hand, if the distance between β phase is relatively large, like in gravity casting (as in the present work), the corrosion rate is increased by β-phase. Influence of the distance between interparticle and/or intermetallics on the corrosion properties of other research areas have also been reported elsewhere [33,34], confirming the similar discussion.

Figure 7 shows potentiodynamic polarization curves of AS11, AS41 and AS91 alloys. Curves for AS21 and AS61 alloys were not included in the figure for clarity but their curves sit between AS11 and AS91 alloys. Corrosion potential (φ_{corr}) and corrosion current density (J_{corr}) values obtained from potentiodynamic polarization curves are shown Table 3. It was noted that the φ_{corr} values of the alloys tend to have more positive values and their J_{corr} values increase with increasing their Al content. The difference between J_{corr} value of AS11 and

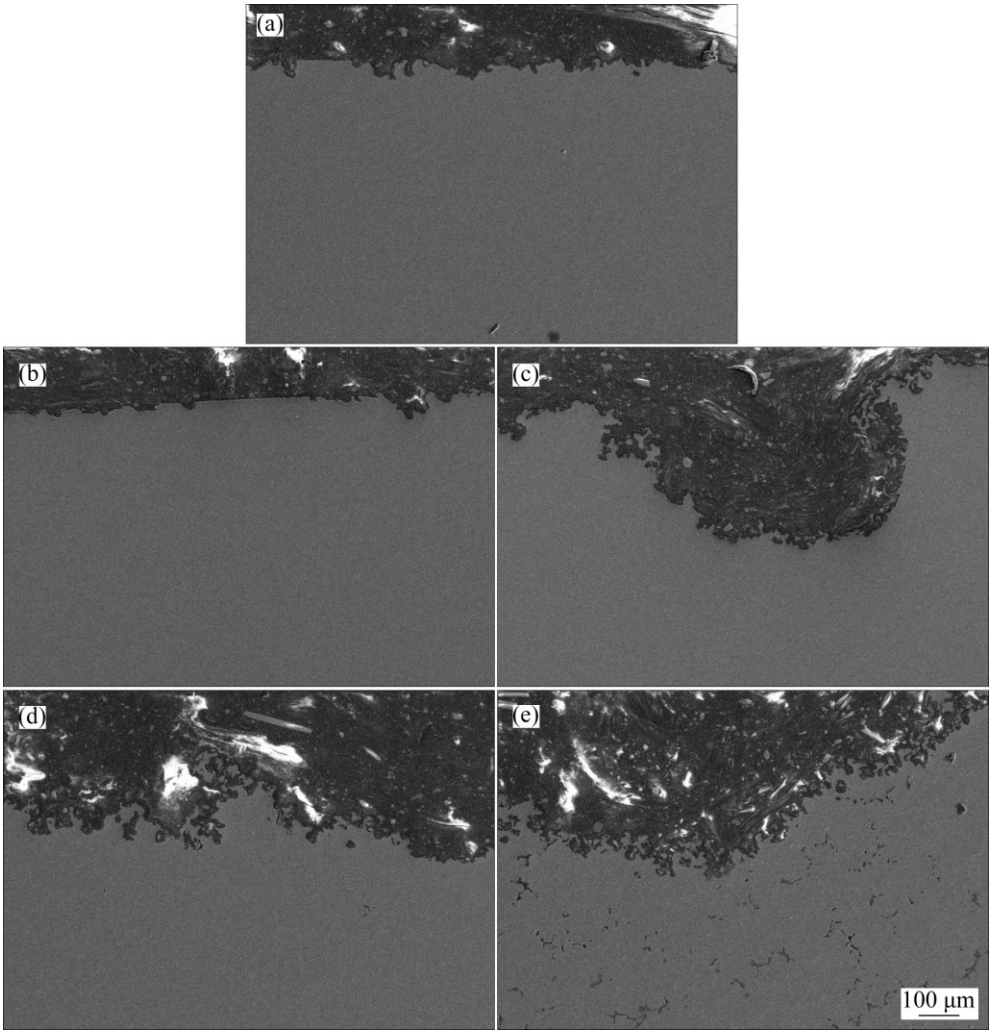

Fig. 6 SEM images showing cross section of AS11 (a), AS21 (b), AS41 (c), AS61 (d) and AS91 (e) Mg alloys exposed to 3.5% NaCl for 72 h

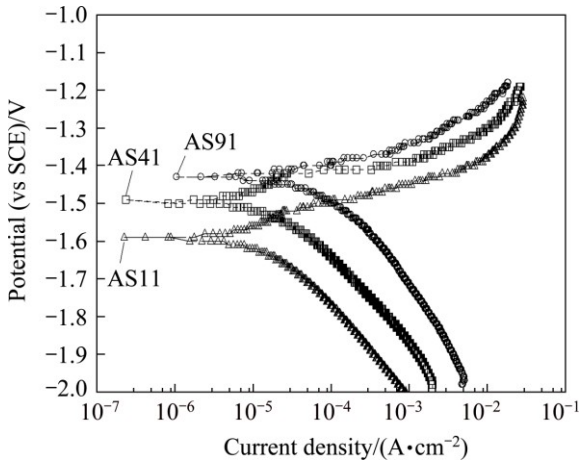

Fig. 7 Potentiodynamic polarization curves for AS series Mg alloys in 3.5% NaCl environment

AS21 is considerably small (i.e., 5.43 and 4.72 μA/cm^2, respectively) while it increases nearly 6-fold for AS21 and AS91 alloy (i.e., 4.72 and 27.7 μA/cm^2, respectively). The results in Table 3 are in line with the corrosion loss results in Fig. 5.

Table 3 φ_{corr}, J_{corr} and CR values of AS series Mg alloys derived from polarization curves

Alloy	φ_{corr}/mV	J_{corr}/(μA·cm^{-2})	CR (mpy)
AS11	−1591	5.43	7.05
AS21	−1497	4.72	6.34
AS41	−1493	6.87	8.58
AS61	−1365	8.79	10.12
AS91	−1430	27.70	45.98

Figures 8(a)−(e) show surfaces of the examined alloys covered by a film after 1 h immersion in 3.5% NaCl environment. It is clear that the surface of AS21 and AS41 alloys (Figs. 8(b) and (c)) are fully covered by the film while the continuity of the film is interrupted by the β and the Mg_2Si phases in AS61 and AS91 alloys owing to coarsening of the phases (Figs. 8(d) and (e)). It is well known that the film on the surface of Mg and its alloys is formed as quasi-passive form of $Mg(OH)_2$. This $Mg(OH)_2$ film is porous [35] and not fully protective, therefore, it is destroyed because of existence of Cl^- at prolonged exposure time, forming the electrochemical reaction [36]:

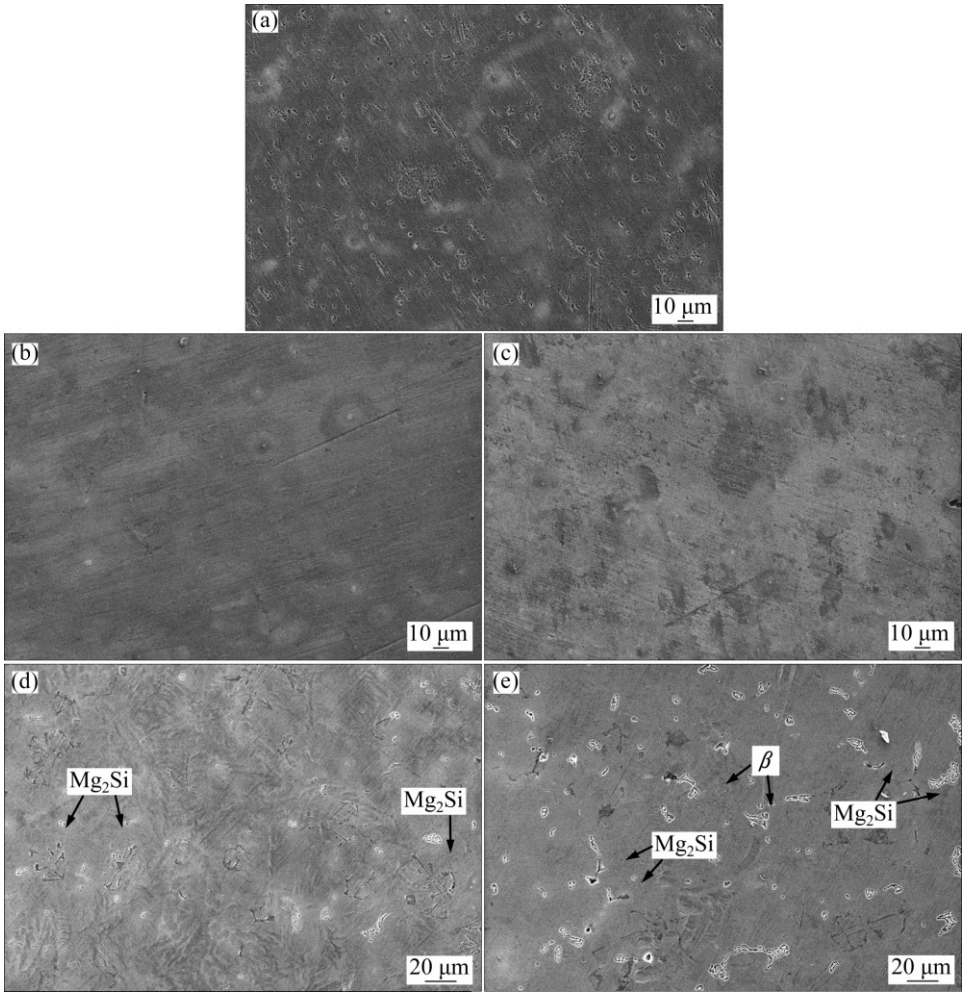

Fig. 8 Surface morphologies showing oxide film on AS11 (a), AS21 (b), AS41 (c), AS61 (d) and AS91 (e) alloys exposed to 3.5% NaCl for 1 h (Arrows show examples of corrosion sites induced by β and Mg_2Si intermetallic phases)

$$2Mg^{2+}(aq)+4H_2O+3OH^-(aq)+Cl^-(aq)\rightarrow Mg_2(OH)_3C1\cdot 4H_2O(s) \quad (1)$$

The corrosion products ($Mg_2(OH)_3Cl\cdot 4H_2O$) provide a protective layer, preventing oxygen and other corrosion media and thereby decreasing corrosion rate in the later corrosion process [36].

The corrosion of AS series alloys can be explained as: the first is the film on the surface of Mg alloys and the second is the morphology of intermetallics (β and Mg_2Si) influenced by Al addition. SONG and ATRENS [37] proposed formation of oxide film on AZ91 alloys. The film consisted of three layers: an inner layer (rich in Al_2O_3), a middle layer (mainly MgO) and an outer layer ($Mg(OH)_2$). More recently, the work of ESMAILY et al [38] showed that Al enrichment in the inner part of the film on AZ91 alloy was evident and the Al was in the oxidized state. Both SONG and ATRENS [37] and ESMAILY et al [38] suggested the positive effect of Al in Mg alloy on corrosion properties was due to the protective properties of the Al-enriched layer at the inner part of the film (i.e., Al_2O_3 layer at the inner part may act as a passive film between the quasi-passive film and the surface of the alloy). Compared to AS11 alloy, better corrosion resistance of AS21 alloy could be due to increased Al content of Mg alloy. It is obvious that the corrosion has initiated from the α-Mg in the vicinity of both β and Mg_2Si intermetallics as shown in Figs. 8(d) and (e). Although, Al contents of AS41, AS61 and AS91 alloys are higher than those of AS11 and AS21 alloys, their higher corrosion loss may be due to discontinuity of the oxide film on the regions where relatively coarsened β and Mg_2Si intermetallics are present. As discussed earlier in the microstructure section, the presence of β phase increases and its morphology coarsens as Al content of the alloy increases. Based on galvanic corrosion principles [30], a higher amount of cathode (intermetallics) in relation to the size of the anode (α-Mg) results in an increased galvanic corrosion. A recent report [15] has revealed that Mg_2Si acts as a local cathode in AS31 alloy and thus promotes the dissolution of surrounding α-Mg phase. Contrarily, other works [39,40] have reported that Mg_2Si has little deleterious or negligible effect on the corrosion of α-Mg phase since the electrochemical potential of the Mg_2Si precipitate (−1.65 V (vs SCE)) is similar to that of magnesium (−1.66 V (vs SCE)). Although, Mg_2Si phase has little deleterious effect from the electrochemical potential point of view, interruption of the continuity of the oxide film on the surface of the alloy, owing to formation of blocky and/or Chinese-script type Mg_2Si intermetallics, is evident as shown in Figs. 8(d) and (e). Such phenomenon in AS series Mg alloys seems not to have been reported in literature. Relatively massive intermetallic phases may not be covered fully with protective oxide film on the α-Mg alloy. Regions of the interrupted areas may result in an additional corrosion sites in addition to the β phase propagated corrosion. Indeed, the corrosion had been initiated near the Mg_2Si intermetallics as shown in Figs. 8(d) and (e). SRINIVASAN et al [32] reported that fine and evenly distributed polygon shaped Mg_2Si intermetallic precipitates effectively inhibited the corrosion, compared to the coarse Chinese-script Mg_2Si in AZ91 alloy. In the present work, fine and evenly distributed Mg_2Si phases, present in AS11 and AS21 alloys, presented the best corrosion resistance in accord with SRINIVASAN et al [32]. The present study indicated that Al content of gravity cast AS series Mg alloys should be below 4% in order to avoid coarsening of β and Mg_2Si intermetallics. The coarsened intermetallics may cause the interruption of continuation of the oxide film on the surface as well as propagation of the corrosion by following the intermetallic network in the microstructure.

4 Conclusions

1) Microstructure of the AS series Mg alloys was composed of α-Mg matrix, $Mg_{17}Al_{12}$ (β) and Mg_2Si intermetallic phases. Presence of β phase was negligible in AS11 and AS21 alloys whereas its content increased in an increasing order for AS41, AS61 and AS91 alloys.

2) As Al content of the alloys increased (>4%), the globular shape β phase was transformed into a more coarsened lamellar or partially divorced β eutectics.

3) The Mg_2Si intermetallic precipitates dispersed as fine particles and needle-like Chinese-script in the microstructure of AS11 and AS21 alloys whereas these precipitates appeared as massive particles and bold Chinese-script type intermetallics in the microstructure of AS41, AS61 and AS91 alloys.

4) The results from both the immersion tests and the potentiodynamic polarization measurements showed that AS11 and AS21 alloys exhibited much better corrosion resistance compared with those of the AS41, AS61 and AS91 alloys.

5) The corrosion attack at the samples made of AS91 is tremendous which was attributed to the influence of the morphology of β phase and the interruption of continuity of oxide film on the surface of the alloys owing to coarsened β and Mg_2Si phases.

References

[1] FRIEDRICH H E, MORDIKE B L. Magnesium technology metallurgy, design data, applications [M]. Berlin: Springer-Verlag, 2006.

[2] LUO A A, SACHDEV A K. Applications of magnesium alloys in automotive engineering [C]//C BETTLES, M BARNETT. Wrought

Magnesium Alloys. Sawston, Cambridge: Woodhead Publishing, 2012: 393−426.

[3] PEKGULERYUZ M. Alloying behavior of magnesium and alloy design [C]//M O PEKGULERYUZ, K U KAINER, A A KAYA. Fundamentals of Magnesium Alloy Metallurgy. Sawston Cambridge: Woodhead Publishing, 2013: 152−196.

[4] KING J F. Development of practical high temperature magnesium casting alloys [C]//Magnesium Alloys and their Applications. Weinhein, Germany: Wiley-VCH, 2000: 14−22.

[5] NAYEB-HASHEMI A A, CLARK J B. Phase diagrams of binary magnesium alloys [M]. Ohio: ASM Intl, 1998.

[6] KIM B H, LEE S W, PARK Y H, PARK I M. The microstructure, tensile properties, and creep behavior of AZ91, AS52 and TAS652 alloy [J]. Journal of Alloys and Compounds, 2010, 493: 502−506.

[7] BLUM W, ZHANG P, WATZINGER B, GROSSMANN B V, HALDENWANGER H G. Comparative study of creep of the die-cast Mg-alloys AZ91, AS21, AS41, AM60 and AE42 [J]. Materials Science and Engineering A, 2001, 319−321: 735−740.

[8] EVANGELISTA E, GARIBOLDI E, LOHNE O, SPIGARELLI S. High-temperature behaviour of as die-cast and heat treated Mg−Al−Si AS21X magnesium alloy [J]. Materials Science and Engineering A, 2004, 387−389: 41−45.

[9] ZHANG P. Creep behavior of the die-cast Mg−Al alloy AS21 [J]. Scripta Materialia, 2005, 52: 277−282.

[10] RUDAJEVOVÁ A, LUKÁČ P. Comparison of the thermal properties of AM20 and AS21 magnesium alloys [J]. Materials Science and Engineering, 2005, 397: 16−21.

[11] AKYUZ B. Influence of aluminum content on machinability of AS series cast magnesium alloys [J]. Transactions of Nonferrous Metals Society of China, 2014, 24: 3452−3458.

[12] SENF J, BROSZEIT E, GUGAU M, BERGER C. Corrosion and galvanic corrosion of die casted magnesium alloys [C]//H I KAPLAN, J HRYN, B CLOW. Magnesium Technology 2000. Nashville, TN: TMS, 2000: 136−142.

[13] ZUCCHI F, GRASSI V, FRIGNANI A, TRABANELLI G. Corrosion behaviour of untreated and termally-treated AS21x Mg Alloy in sulphate and chloride media [C]//Proceedings of 16th International Corrosion Congress, China: International Corrosion Council, 2005.

[14] ELSAWY E N, EL-SAYED H A, EL SHAYEB H A. Corrosion of Mg, AS31 and AZ91 alloys in nitrate solutions [J]. Journal of Alloys and Compounds, 2010, 492: 69−76.

[15] GUPTA R K, SUKIMAN N L, FLEMING K M, GIBSON M A, BIRBILIS N. Electrochemical behavior and localized corrosion associated with Mg_2Si particles in Al and Mg Alloys [J]. ECS Electrochemistry Letters, 2012, 1: B1−B3.

[16] CANDAN S, UNAL M, TURKMEN M, KOC E, TUREN Y, CANDAN E. Improvement of mechanical and corrosion properties of magnesium alloy by lead addition [J]. Materials Science and Engineering A, 2009, 501: 115−118.

[17] CANDAN S, UNAL M, KOC E, TUREN Y, CANDAN E. Effects of titanium addition on mechanical and corrosion behaviours of AZ91 magnesium alloy [J]. Journal of Alloys and Compounds, 2011, 509: 1958−1963.

[18] ZHANG Xin, LI Yong-jun, ZHANG kui, WANG Chang-shun, LI Hong-wei, MA Ming-long, ZHANG Bao-dong. Corrosion and electrochemical behavior of Mg−Y alloys in 3.5% NaCl solution [J]. Transactions of Nonferrous Metals Society of China, 2013, 23: 1226−1236.

[19] ZENG Rong-chang, ZHANG Jin, HUANG Wei-jiu, DIETZEL W, KAINER K U, BLAWERT C, KE Wei. Review of studies on corrosion of magnesium alloys [J]. Transactions of Nonferrous Metals Society of China, 2006, 16: 763−771.

[20] GUSIEVA K, DAVIES C H J, SCULLY J R, BIRBILIS N. Corrosion of magnesium alloys: The role of alloying [J]. International Materials Reviews, 2015, 60: 169−194.

[21] LI X L, CHEN Y B, WANG X, MA G R. Effect of cooling rates on as-cast microstructures of Mg−9Al−xSi (x=1, 3) alloys [J]. Transactions of Nonferrous Metals Society of China, 2010, 20: 393−396.

[22] CANDAN S, CELIK M, CANDAN E. Effectiveness of Ti-micro alloying in relation to cooling rate on corrosion of AZ91 Mg Alloy [J]. Journal of Alloys and Compounds, 2016, 672: 197−203.

[23] PEKGULERYUZ M O, KAYA A A. Creep resistant magnesium alloys for powertrain applications [J]. Advanced Engineering Materials, 2003, 5: 866−878.

[24] BRONFIN B, KATSIR M, AGHION E. Preparation and solidification features of AS21 magnesium alloy [J]. Materials Science and Engineering A, 2001, 302: 46−50.

[25] CHENG Y L, QIN T W, WANG H M, ZHANG Z. Comparison of corrosion behaviors of AZ31, AZ91, AM60 and ZK60 magnesium [J]. Transactions of Nonferrous Metals Society of China, 2009, 19: 517−524.

[26] KOC E. An investigation on corrosion dependent mechanical behaviours of biodegradable magnesium alloys [D]. Karabuk: Karabuk University, Institute of Science and Technology, 2013.

[27] BOBY A, SRINIVASAN A, PILLAI U T S, PAI B C. Mechanical characterization and corrosion behavior of newly designed Sn and Y added AZ91 alloy [J]. Materials and Design, 2015, 88: 871−879.

[28] MA G R, LI X L, XIAO L, LI Q F. Effect of holding temperature on microstructure of an AS91 alloy during semisolid isothermal heat treatment additions [J]. Journal of Alloys and Compounds, 2010, 496: 577−581.

[29] ZHENG W C, LI S S, TANG B, ZENG D B. Microstructure and properties of Mg−Al binary alloys [J]. China Foundry, 2006, 3: 270−274.

[30] SONG G, ATRENS A, DARGUSCH M. Influence of microstructure on the corrosion of die cast AZ91D [J]. Corrosion Science, 1999, 41: 249−273.

[31] SONG G. Investigation on corrosion of magnesium and its alloys [J]. Journal Corrosion Science and Engineering, 2003, 6: C104.

[32] SRINIVASAN A, NINGSHEN S, MUDALI U, PILLAI U T S, PAI B C. Influence of Si and Sb additions on the corrosion behavior of AZ91 magnesium alloy [J]. Intermetallics, 2007, 15: 1511−1517.

[33] CANDAN S. Effect of SiC particle size on corrosion behavior of pressure infiltrated Al matrix composites in a NaCl solution [J]. Materials Letters, 2004, 58: 3601−3605.

[34] CANDAN S. An investigation on corrosion behaviour of pressure infiltrated Al−Mg alloy/SiC_p composites [J]. Corrosion Science, 2009, 51: 1392−1398.

[35] GHALI E. Corrosion resistance of aluminum and magnesium alloys, understanding, performance and testing [M]. New Jersey: Wiley Publishing, 2010.

[36] LIN C, LI X. Role of CO_2 in the initial stage of atmospheric corrosion of AZ91 magnesium alloy in the presence of NaCl [J]. Rare Metals, 2006, 25: 190−196.

[37] SONG G, ATRENS A. Corrosion mechanisms of magnesium alloys [J]. Advanced Engineering Materials, 1999, 1: 11−33.

[38] ESMAILY M, BLUCHER D B, SVENSSON J E, HALVARSSON M, JOHANSSON L G. New insights into the corrosion of magnesium alloys−The role of aluminum [J]. Scripta Materialia, 2016, 115: 91−95.

[39] NA Y G, ELIEZER D, SHIN K S. Corrosion of new wrought magnesium alloys [J]. Material Science Forum, 2005, 488−489: 839−844.

[40] CARLSON B E, JONES J W. The metallurgical aspects of the corrosion behaviour of cast Mg−Al alloys [C]//Light Metals Processing and Applications. Quebec: Metallurgical Society of the Canadian Institute of Mining, Metallurgy and Petroleum, 1993: 833−847.

Mg−Al−Si 合金腐蚀的对比研究

Sennur CANDAN[1], Ercan CANDAN[2]

1. Department of Mechanical and Manufacturing Engineering,
Bilecik Seyh Edebali University, Bilecik 11210, Turkey;
2. Department of Mechanical Engineering, Avrasya University, Trabzon 61200, Turkey

摘　要：系统研究在相同冷却条件和成分控制条件下，不同 Mg−Al−Si 合金(AS11，AS21，AS41，AS61 和 AS91)的腐蚀行为。采用光学显微镜和扫描电子显微镜观察合金的显微组织。采用浸泡实验和动电位极化测试研究合金在 3.5% NaCl 溶液中的腐蚀行为。结果表明，添加 2.0% Al(质量分数)的合金(AS21)抗腐蚀能力提高，而 Al 含量大于 2.0%(AS41，AS61，AS91)时，合金的抗腐蚀能力降低。这是由于生成了 β 相作为阴极，以及 β 相和 Mg_2Si 相的粗化导致合金表面氧化膜的破裂后不连续。

关键词：镁合金；AS 系列合金；显微组织；腐蚀

(Edited by Yun-bin HE)